

Structural evolution and bandgap modulation of layered β-$GeSe_2$ single crystal under high pressure

Hengli Xie(谢恒立), Jiaxiang Wang(王家祥), Lingrui Wang(王玲瑞), Yong Yan(闫勇), Juan Guo(郭娟), Qilong Gao(高其龙), Mingju Chao(晁明举), Erjun Liang(梁二军), and Xiao Ren(任霄)

Citation: Chin. Phys. B, 2022, 31 (**7**): 076101. DOI: 10.1088/1674-1056/ac6db8
Journal homepage: http://cpb.iphy.ac.cn; http://iopscience.iop.org/cpb

What follows is a list of articles you may be interested in

Raman spectroscopy investigation on the pressure-induced structural and magnetic phase transition in two-dimensional antiferromagnet $FePS_3$

Hong Zeng(曾鸿), Tingting Ye(叶婷婷), Peng Cheng(程鹏), Deyuan Yao(姚德元), and Junfeng Ding(丁俊峰)
Chin. Phys. B, 2022, 31 (**5**): 056109. DOI: 10.1088/1674-1056/ac5a41

Temperature dependence of bismuth structures under high pressure

Xiaobing Fan(范小兵), Shikai Xiang(向士凯), and Lingcang Cai(蔡灵仓)
Chin. Phys. B, 2022, 31 (**5**): 056101. DOI: 10.1088/1674-1056/ac398d

Dependence of nitrogen vacancy color centers on nitrogen concentration in synthetic diamond

Yong Li(李勇), Xiaozhou Chen(陈孝洲), Maowu Ran(冉茂武), Yanchao She(佘彦超), Zhengguo Xiao(肖政国), Meihua Hu(胡美华), Ying Wang(王应), and Jun An(安军)
Chin. Phys. B, 2022, 31 (**4**): 046107. DOI: 10.1088/1674-1056/ac3220

Pressure dependence of the thermal stability in $LiMn_2O_4$

Yan Zeng(曾彦), Hao Liang(梁浩), Shixue Guan(管诗雪), Junpu Wang(王俊普), Wenjia Liang(梁文嘉), Mengyang Huang(黄梦阳), and Fang Peng(彭放)
Chin. Phys. B, 2022, 31 (**1**): 016104. DOI: 10.1088/1674-1056/ac1932

Prediction of scandium tetraboride from first-principles calculations: Crystal structures, phase stability, mechanical properties,and hardness

Bin-Hua Chu(初斌华) and Yuan Zhao(赵元)
Chin. Phys. B, 2021, 30 (**7**): 076107. DOI: 10.1088/1674-1056/abe116

Structural evolution and bandgap modulation of layered β-$GeSe_2$ single crystal under high pressure

Hengli Xie(谢恒立)[1], Jiaxiang Wang(王家祥)[1], Lingrui Wang(王玲瑞)[1], Yong Yan(闫勇)[2], Juan Guo(郭娟)[1], Qilong Gao(高其龙)[1], Mingju Chao(晁明举)[1], Erjun Liang(梁二军)[1], and Xiao Ren(任霄)[1,†]

[1] *Key Laboratory of Materials Physics of Ministry of Education, School of Physics and Microelectronics, Zhengzhou University, Zhengzhou* 450052, *China*

[2] *College of Physics and Materials Science, Henan Normal University, Xinxiang* 453007, *China*

(Received 28 March 2022; revised manuscript received 3 May 2022; accepted manuscript online 7 May 2022)

Germanium diselenide ($GeSe_2$) is a promising candidate for electronic devices because of its unique crystal structure and optoelectronic properties. However, the evolution of lattice and electronic structure of β-$GeSe_2$ at high pressure is still uncertain. Here we prepared high-quality β-$GeSe_2$ single crystals by chemical vapor transfer (CVT) technique and performed systematic experimental studies on the evolution of lattice structure and bandgap of β-$GeSe_2$ under pressure. High-precision high-pressure ultra low frequency (ULF) Raman scattering and synchrotron angle-dispersive x-ray diffraction (ADXRD) measurements support that no structural phase transition exists under high pressure up to 13.80 GPa, but the structure of β-$GeSe_2$ turns into a disordered state near 6.91 GPa and gradually becomes amorphous forming an irreversibly amorphous crystal at 13.80 GPa. Two Raman modes keep softening abnormally upon pressure. The bandgap of β-$GeSe_2$ reduced linearly from 2.59 eV to 1.65 eV under pressure with a detectable narrowing of 36.5%, and the sample under pressure performs the piezochromism phenomenon. The bandgap after decompression is smaller than that in the atmospheric pressure environment, which is caused by incomplete recrystallization. These results enrich the insight into the structural and optical properties of β-$GeSe_2$ and demonstrate the potential of pressure in modulating the material properties of two-dimensional (2D) Ge-based binary material.

Keywords: high pressure, structural phase transition, Raman spectroscopy scattering, layered material

PACS: 61.50.Ks, 07.35.+k, 78.30.–j, 63.22.Np **DOI:** 10.1088/1674-1056/ac6db8

1. Introduction

Recently, the exploration of the relationship between structure and properties of two-dimensional (2D) materials has become the focus of research.[1–5] This is attributed to the promising applications of 2D materials in field-effect transistors,[6–8] photodetectors,[9,10] and electrocatalysts,[11] *etc.* To further develop the applications of 2D materials, it is necessary to break through the intrinsic structure of the materials and to discover, characterize, and control the crystal structure and property changes of 2D materials.[12–14] For example, relying on the structural phase transition of metal dichalcogenides (TMDs) materials (MoS_2,[12] $MoTe_2$,[15] and WS_2[16]) from the semiconductor phase (2H) to the metallic phase (1T, 1T′), 2D electronic devices with low contact resistance could be fabricated accompanying high carrier mobility, high switching rate, and superior electrocatalytic performance.[17,18] Therefore, how to effectively regulate the structure of 2D materials to develop more potential applications remains attractive.

As a powerful experimental method for revealing the effects of atomic and electronic structure changes on the electronic and optoelectronic properties, pressure is the best candidate to modulate the structure in 2D materials without introducing impurities and damages.[19–22] For example, the exciton binding energy of 2D perovskites is reduced and the photocurrent is significantly enhanced under pressure.[23] Furthermore, TMDs exhibit specific physical phenomena such as metallization and superconductivity under pressure.[24–28] Therefore, it is significant to explore the tunability of the lattice and electronic structures of 2D materials by pressure to get more insight into their intrinsic structural properties.

Germanium diselenide (β-$GeSe_2$) plays an essential role in the family of 2D Ge-based binary materials.[29] Relying on its direct wide bandgap of 2.74 eV,[30,31] weak interlayer interaction,[32] and good air stability,[31] β-$GeSe_2$ could be used in the fields of ultraviolet photoelectric detection,[33] infrared waveguides,[34] polarization-sensitive photodetection,[30,31] and storage units.[35] Since it performs well in many applications at atmospheric pressure, it is necessary to reveal the behavior of lattice and electronic structures under high pressure and to explore its more potential applications under extreme conditions. Actually, many efforts have been made to uncover the lattice and electronic structure evolution of β-$GeSe_2$ under high pressure, but many controversies still remain.

In experiments, Popović *et al.* utilized high-pressure Raman scattering to demonstrate that β-$GeSe_2$ exhibited amorphization at 6.20 GPa and transformed to α-$GeSe_2$ upon fur-

†Corresponding author. E-mail: rxphy@zzu.edu.cn

© 2022 Chinese Physical Society and IOP Publishing Ltd

ther compression to 7.00 GPa, then back to amorphization when the pressure continuously increased to 8.00 GPa.[36] However, another pressure-dependent Raman experiment by Andrzej Grzechnik *et al.* speculated that β-$GeSe_2$ partially broke at 7.00 GPa and the bilaterally shared Ge_2Se_8 tetrahedra began to break locally, forming a local HgI_2-type structure. Furthermore, their high-pressure energy dispersive x-ray diffraction supported that β-$GeSe_2$ at 11.00 GPa was completely amorphous and no structural phase transition existed during pressuring to 14.00 GPa.[37] In addition to the experiments, the local density approximation (LDA) and generalized gradient approximation (GGA) calculations supported theoretically that the structure of β-$GeSe_2$ suffered Tl-cristobalite-type at 0.52 GPa, HgI_2-type at 2.30 GPa, and CdI_2-type at 3.56 GPa.[38] While another *ab initio* calculation depicted the onset of CdI_2-type as 18.50 GPa.[39] Accordingly, as outlined above, there are still a lot of controversies on the lattice evolution of β-$GeSe_2$ in the experimental and theoretical results.

In this work, we have synthesized high-quality single crystals of β-$GeSe_2$ by the chemical vapor transfer (CVT) experimental method. We apply symmetric diamond anvil cell (DAC) high-pressure technique for in situ angle-dispersive x-ray diffraction (ADXRD), ultra low frequency (ULF) Raman scattering, and UV-vis absorption experiments to obtain the effect of pressure on the lattice and electronic structure of β-$GeSe_2$. Our results approve that no structural phase transition exists as pressure increases to 13.80 GPa but the structure becomes disorder at 6.91 GPa and turns into the amorphous state at 13.80 GPa. Some phonon energies show inconsistency at 6.91 GPa, indicating that the inter-layer interactions play a more significant role for the phonon energy than intra-layer interactions for some certain phonons. Two Raman modes depict softening behaviors over a large pressure range, which could be attributed to the weak intramolecular bonds. This phenomenon is accord with the solid hydrogen and GeP_5 up to high pressure.[40,41] The electronic bandgap of β-$GeSe_2$ decreases linearly with increasing pressure signifying that no electronic phase transition appears. The color variation of the sample with pressure was captured in real-time, changing from bright yellow to dark red and finally to black. Our ADXRD and UV-vis absorption experiments prove the existence of an incomplete recrystallization process in β-$GeSe_2$.

2. Experimental details

2.1. Synthesis of β-$GeSe_2$ single crystals

The bulk β-$GeSe_2$ single crystals were synthesized in a dual-temperature zone tube slide furnace by chemical vapor transfer (CVT) reaction technique. Analytical grade reagents of GeSe (purity 99.999%) and Se (Aladdin in purity 99.999%) powders were used as raw materials based on the chemical stoichiometry of β-$GeSe_2$ (Fig. 1). Firstly, two crucibles separately containing GeSe (0.01 mol) and Se (0.01 mol) powders were placed in the quartz tube, 4 cm and 20 cm from the left side away from the first heating center respectively. After the quartz tube was vacuumized to −0.1 MPa, the high-purity Ar gas was filled into the quartz tube until the pressure in the tube returned to atmospheric pressure. This process of gas washing was repeated three times. Then the quartz tube was purged with Ar gas for 60 min with a flow rate of 200 sccm to ensure that no air existed in the quartz tube before the quartz tube was heated up. The left and right temperature zone of the quartz tube was set as 720 °C and 710 °C with a rate of 10 °C/min, separately. Once the temperature of the left zone reached 720 °C, the furnace needs to be moved to the left by 4 cm timely to ensure that the two raw materials could achieve sublimation point simultaneously. Meanwhile, the Ar gas with 200 sccm was replaced by the mixed gas of 90% Ar and 10% H_2 with a rate of 40 sccm. The whole reaction process was kept for 25 min, then the tube was cooled to room temperature at a cooling rate of 2 °C/min. Then, the high-quality single crystals β-$GeSe_2$ with bright yellow flake were obtained.

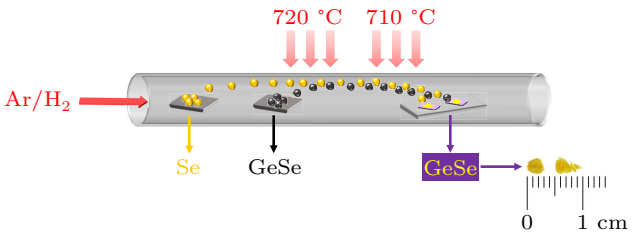


Fig. 1. Sketch of preparation equipment of β-$GeSe_2$ single crystal by CVT method.

2.2. High-pressure generation

A symmetric DAC was used for high-pressure experiments, and the culet size of the diamond anvils was 400 μm. The sample was loaded into a 150-μm diameter hole of the T301 stainless steel gasket, which was pre-pressed to a thickness of 40 μm. A small ruby ball was placed in the sample compartment for in situ pressure calibration, utilizing the standard ruby fluorescence method. Silicone oil was used as the pressure transmitting medium for high-pressure experiments.

2.3. *In situ* high-pressure measurements

In situ high-pressure ADXRD experiments at a wavelength of 0.6199 Å beam were carried out at beamline Unit BL15U1, Shanghai Synchrotron Radiation Facility (SSRF), China. CeO_2 was used as the standard sample to do the calibration. The collected 2D images were integrated based on the FIT2D program to obtain a plot of one-dimensional (1D) intensity *versus* diffraction angle 2-theta patterns. The Reflex module of Materials Studio was used to refine the XRD patterns.

Pressure-dependent Raman spectra were collected with Horiba Jobin Yvon LabRAM HR Evolution Raman spectrom-

eter in a backscattering configuration equipped with 1800-g/mm grating. BragGrate notch filters allow for measurements down to about 10 cm^{-1}. A semiconductor refrigeration CCD detector with a focal length of 800 mm after gratings provides a high energy resolution of 0.6 cm^{-1}. The incident laser with a wavelength of 633 nm originating from an He–Ne laser was used for excitation. To reduce the influence of laser heating on the sample, the laser power was lower than 0.15 mW.

In situ high-pressure optical absorption spectra measurement was performed between 250 nm and 1000 nm using a deuterium–halogen light source and recorded with an optical fiber spectrometer (Ocean Optics, QE65000). Each new acquisition was performed after a few minutes as pressure rise to a certain value, which will intrinsically explain any kinetic dependence of the measurement process. The transmission spectrum of silicon oil around the sample was subtracted as the background.

3. Results and discussion

3.1. High precision pressure-dependent Raman spectroscopy revealing structural evolution and pressure limit of β-$GeSe_2$

$GeSe_2$ crystallizes in three phases, including orthorhombic α-$GeSe_2$ (space group $Pmmn$), monoclinic β-$GeSe_2$ (space group $P2_1/c$), and hexagonal γ-$GeSe_2$ (space group $P\bar{3}m1$).[38] All three structures are layered. In particular, β-$GeSe_2$ is the most stable form with the lowest energy among the three phases.[31,38] The crystal structure basic unit of β-$GeSe_2$ is a $GeSe_4$ tetrahedron. Every unit cell has two layers and van der Waals forces along the z axis separate the layers.[32] Each layer is composed of parallel chains of corner-sharing $GeSe_{4/2}$ tetrahedra (CST) along the a axis and interconnected by pairs of edge-sharing Ge_2Se_8 double tetrahedra (EST) along the b axis (Fig. 2).[30]

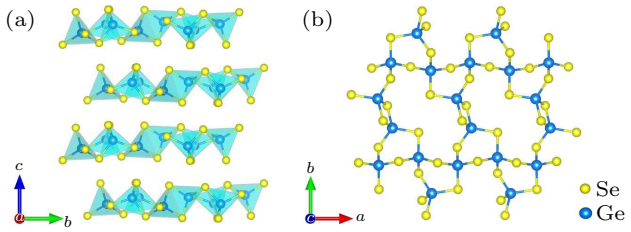


Fig. 2. Crystal structure of β-$GeSe_2$ from side (a) and top (b) view.

A situ high-pressure Raman scattering is performed to study the modification of structure under the pressure of β-$GeSe_2$. The group theory analysis provides the irreducible representations of β-$GeSe_2$ that could rule the vibrational patterns of phonon at Γ point of the Brillouin zone as the following equation:

$$\Gamma = 36A_g + 36B_g + 36A_u + 36B_u, \quad (1)$$

where A_g and B_g phonons are Raman-active modes with the symmetric center of vibrations, while A_u and B_u are infrared (IR)-active modes with no symmetric vibrational center. Our single crystal sample of β-$GeSe_2$ for Raman testing is a bulk material and the highest symmetric axis is along the b-axis direction.[36] Thus the Z direction in the phonon selection rule is the b axis.[42] In order to best detect the A_g and B_g phonons, the incident and scattered light polarizations to obey the phonon selection rule. For example, part of A_g modes could be obtained when the incident and scattered light polarizations are parallel to the a axis. If we put the a axis along the X direction, the configuration above could be noted as $XX(aa)$. According to this naming method, A_g modes could be detected under $XX(aa)$, $YY(cc)$, $XY(ac)$, and $ZZ(bb)$ polarizations. B_g modes could be obtained by $XZ(ab)$ and $YZ(cb)$ polarizations. For the texture of β-$GeSe_2$ single crystal is soft, it is difficult to obtain ac or bc plane and only the experimental measurements on the ab plane could be available. Therefore, we just obtain partial A_g and B_g modes. Figure 3 shows our room temperature and ambient pressure Raman spectra under polarized laser configuration on the ab plane. 33 branches of A_g modes and 31 branches of B_g modes have been detected successfully (Fig. 3) and the other no detectable branches, 3 branches of A_g modes and 5 branches of B_g modes, may originate from $YY(cc)$ and $XY(ac)$ polarizations in ac plane or cannot be explored due to their low intensities.

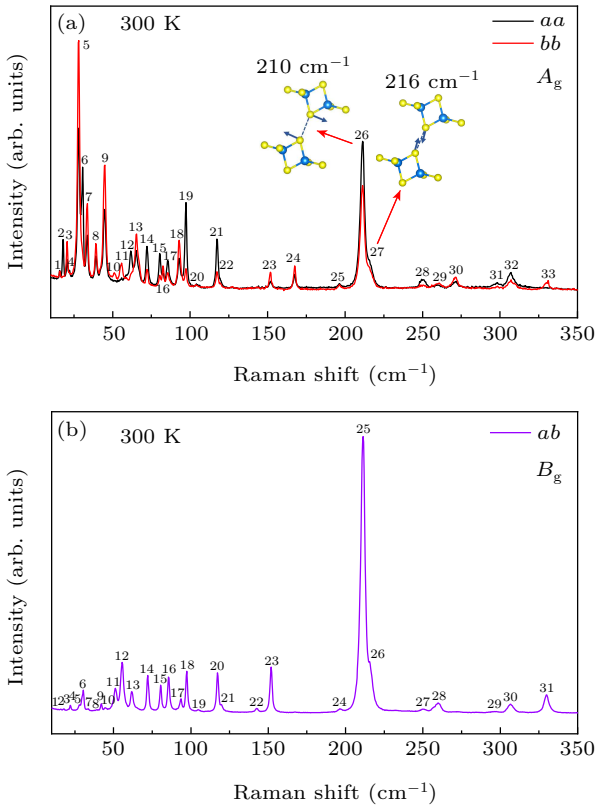


Fig. 3. Polarized Raman spectrum of β-$GeSe_2$ single crystal with parallel (a) and vertical (b) polarization at room temperature and ambient pressure. The inset in Fig. 3(a) shows the atomic vibration patterns of 210 cm^{-1} and 216 cm^{-1}, respectively.

We denote the Raman peaks of A_g and B_g modes at atmospheric pressure and room temperature clearly in Fig. 3 and specific phonon energies are performed in Table S1 in supporting information. It is worth noting that most of A_g and B_g modes stand similarly, which is consistent with the previous Raman research.[43] Compared with the previous results, the Raman peaks we obtained at atmospheric pressure and room temperature are more accurate and complete, which provides more information for the structural analysis of β-$GeSe_2$. The highest Raman peak at 210 cm^{-1} in Fig. 3 is the characteristic peak of β-$GeSe_2$ and could be distinguishable with that of α-$GeSe_2$ at 200 cm^{-1}.[30,44] The dominant peak located at 210 cm^{-1} is assigned to the symmetric breathing vibration mode of the shared-angle $GeSe_4$ tetrahedra and the atomic vibrational pattern of 216 cm^{-1} is also presented (the inset of Fig. 3).[36,37]

The specific variable pressure study of the Raman spectrum of β-$GeSe_2$ is shown in Fig. 4(a), where the pressure is gradually raised in a stepwise fashion up to $\sim$ 13.80 GPa. We fitted all Raman peaks at different pressures except the peaks that were too broad and weak to be fitted. The fitted peak positions are displayed in Fig. S1 in supporting information. It is macroscopically observable that many Raman peaks become broad and seem to merge above 6.91 GPa. We depicted the pressure-dependent full width at half maximum (FWHM) of six peaks that could be well fitted crossing 6.91 GPa (Figs. 4(b)–4(d) and Fig. S2). In Raman experiment, the FWHM reflects the length of the phonon lifetime which could be modulated by the external factors that disturb the intrinsic vibration of phonons.[45] In Figs. 4(b)–4(d) and Fig. S2, it is noticeable that the significant broadening of Raman peaks happen at 6.91 GPa, which is speculated to be caused by a substantial increase in the disorder of the atomic arrangement in the unit cell of β-$GeSe_2$. This is in sync with the previous Raman result that the material shows disorder at 7.00 GPa marked by the indistinguishable peaks at 210 cm^{-1} and 216 cm^{-1}.[37] Resorting to the high resolution of our Raman spectroscopy, as high as 0.6 cm^{-1}, it is obvious that the 210 cm^{-1} (marked by the inverted triangle in Fig. S3) and 216 cm^{-1}(marked by the circle in Fig. S3) peaks always separate in the whole pressure (Fig. S3). Thus, we provide more specific and systematic evidence for the disorder at 7.00 GPa resorting to the abnormal broadening of FWHM at 6.91 GPa than the previous Raman result.[37] In addition, to further demonstrate the effect of the variation of the hydrostatic pressure environment on the experimental results, we also conducted a high-pressure Raman experiment with liquid argon (Ar) as the pressure transfer medium, as shown in Fig. S4. The evolutions of the high-pressure Raman spectra of β-$GeSe_2$ under the two pressure transfer media remain consistent with each other, which proves that if the hydrostatic pressure environment in the DAC changes, the experimental results are unacted.

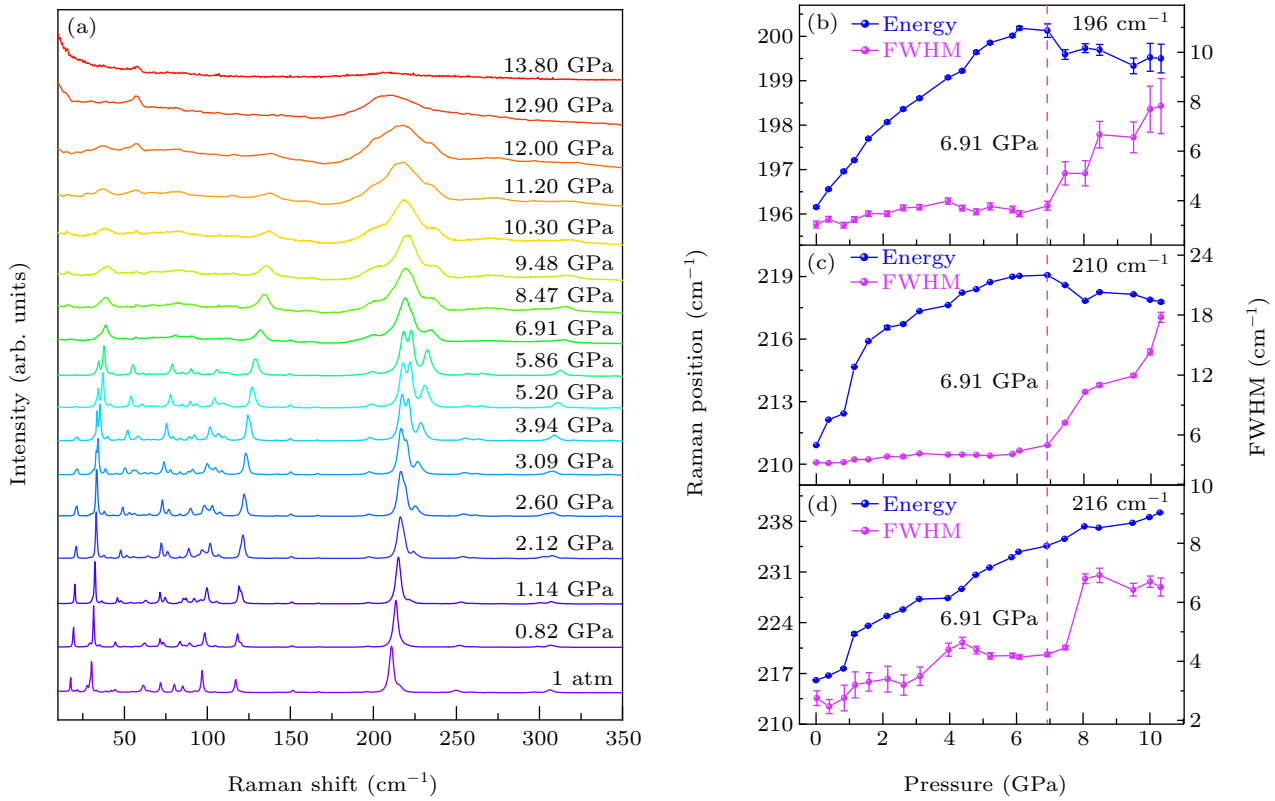


Fig. 4. (a) Variable pressure Raman spectra of β-$GeSe_2$ single crystal with silicone oil as the pressure transfer medium. The pressure-dependent peak energy and FWHM of 196 cm^{-1} (b), 210 cm^{-1} (c), and 216 cm^{-1} (d) peaks.

According to our fitting results, only the Raman peaks at 196 cm^{-1} and 210 cm^{-1} undergo an anomalous redshift at 6.91 GPa (Figs. 4(b) and 4(c)), while the energies of the other four peaks show monotonic changes (Fig. 4(d) and Fig. S2) including the 216-cm^{-1} peaks. In the following part, we will study the reason of the anomaly between 210-cm^{-1} and 216-cm^{-1} peaks. According to the vibrational schematic diagrams in Fig. 3(a), the two Raman peaks at 210 cm^{-1} and 216 cm^{-1} are both contributed by the same Se atoms vibrations, but different vibrational directions. One direction is almost parallel to the Se–Se chain and the other is almost perpendicular to the interlayer Se–Se direction. When the sample turns into disordered at 6.91 GPa, some Ge–Se bonds of the $GeSe_4$ tetrahedron framework would break.[37,46] Thus, we infer that the softening of 210-cm^{-1} peaks is attributed to the Ge–Se bond breaking. The reason why 210-cm^{-1} phonon, not 216-cm^{-1} phonon, softens above 6.91 GPa is that the 210-cm^{-1} phonon involves the Se–Se vibrations along layers while the 216-cm^{-1} phonon is caused by the Se–Se vibration across layers. Due to the bond length decreasing of Se–Se atoms between interlayer upon compression, to a certain extent, it will compensate for the energy loss induced by the Ge–Se bond breaking for 216-cm^{-1} phonon. The monotone increase of 216-cm^{-1} phonon energy demonstrates that the shortening of interlayer spacing, which is a relatively straightforward result of high pressure, has a more obvious effect on the phonon energy than the Ge–Se bond breaking. Therefore, the partial breaking of the Ge–Se bond would not induce a macroscopically structural deformation. To verify our inference, a high-resolution ADXRD experiment that reflects the intrinsic structure evolution of β-$GeSe_2$ needs to be done, which will introduce specifically in the following part.

For the peak at 196 cm^{-1}, with the similar abnormal behavior of 210 cm^{-1}, no explicit vibration modes have been given according to previous studies. Our results (Figs. 4(b) and 4(c)) put forward that the energies of 196-cm^{-1} and 210-cm^{-1} phonons harden respectively 4 cm^{-1} and 9 cm^{-1} from 1 atm (1 atm = 1.01325×10^5 Pa) to 6.91 GPa and soften 0.7 cm^{-1} and 1.4 cm^{-1} from 6.91 GPa to 10.30 GPa. The ratio of 0.7 cm^{-1}/4 cm^{-1} is similar to 1.4 cm^{-1}/9 cm^{-1} indicating that these two phonons have a similar response to pressure. Thus, we conjecture that the abnormal energy change in the 196-cm^{-1} peak is also caused by the partial breaking of the Ge–Se bond like 210-cm^{-1} peak. What is more, the 210-cm^{-1} peak splits at 2.12 GPa (Fig. S3), which could be interpreted as the internal vibrational modes like that in the isomorphic GeS_2.[47]

Apart from the abnormal changes in 210 cm^{-1} and 196 cm^{-1}, the energies of 151-cm^{-1} and 167-cm^{-1} phonons soften from 1 atm to 6.07 GPa above which the peaks are too broad to be fitted with a large error as shown in Fig. 5 and Fig. S5 (The specific fitting diagram is shown in Fig. S6). Different from phonon softening which reflects the structural phase transition at some pressure,[48] our phonon softening behavior upon compression is just like that in solid hydrogen and the layered GeP_5 at high pressure.[40,41] The continuous softening of the two modes may be caused by the elongation of the length of the intra-layer, resulting in the weakening of the intramolecular bonds.

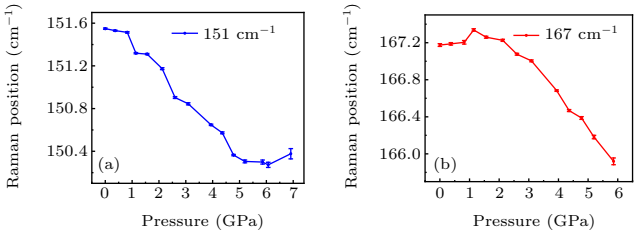


Fig. 5. Pressure-dependent Raman peak positions of 151-cm^{-1} (a) and 167-cm^{-1} (b) peaks.

For purpose of investigating the pressure resistance limit of the β-$GeSe_2$ crystal structure, we applied high pressures of 19.20 GPa to β-$GeSe_2$. According to the Raman spectra in Fig. 4(a), it is clear that the distinguishable Raman peaks exist until 13.80 GPa. Figure 6(a) displays the Raman spectra during decompression from 13.80 GPa, where the Raman characteristic peaks representing the amorphization of β-$GeSe_2$ appeared around 175 cm^{-1}, 199 cm^{-1}, and 216 cm^{-1},[36,49] which signaled that the crystal structure of β-$GeSe_2$ is irreversibly amorphous at 13.80 GPa. The released sample after complete decompression was found to be consistent with that of previously reported glassy $GeSe_2$,[49] implying that the amorphous of $GeSe_2$ induced by pressure possesses the same origin as that prepared at atmospheric pressure, which will provide good insights for understanding and regulating the structure of the $GeSe_2$ glassy state. As shown in Fig. S7(a), when the pressure exceeds 13.80 GPa, the Raman spectra only contain peaks that is similar with the that in 13.80 GPa, which demonstrates only amorphous state exists and β-$GeSe_2$ does not form a new long-range ordered structure near 18.50 GPa. Our conclusion is different from the results predicted by the calculation.[39] Moreover, collecting Raman spectra of the decompression process reveals that the structure of β-$GeSe_2$ does not recover with the decrease of pressure (Fig. S7(b)). If we reduce the maximum pressure to 12.83 GPa, the structure of β-$GeSe_2$ will be restored completely as the pressure is relieved to the ambient pressure (shown in Fig. 6(b)).

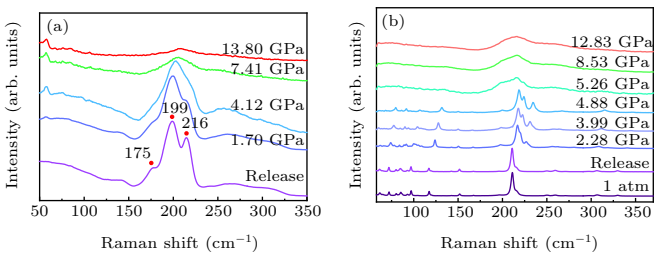


Fig. 6. The decompressed Raman spectra of β-$GeSe_2$ from 13.80 GPa (a) and 12.83 GPa (b) at room temperature.

3.2. ADXRD under high pressure demonstrates no structural phase transition in β-$GeSe_2$ single crystal

Figure 7(a) shows representative ADXRD data of β-$GeSe_2$ during compression to 13.20 GPa and decompression. The Reflex module of Materials Studio was used to refine the XRD patterns. The refinement of ADXRD data at ambient pressure indicates that the intrinsic structure of β-$GeSe_2$ belongs to the monoclinic phase with $P2_1/c$ space group (Fig. S8(a)), which is consistent with previous reports.[32,33] Most diffraction peaks broaden and disappear when the pressure exceeds 7.19 GPa, implying some disorder existing in the structure, which is consistent with our Raman result. Beyond 7.19 GPa, the diffraction peaks still move uniformly with upon to 13.22 GPa implying no obvious amorphization at 13.22 GPa. This could be verified by the ADXRD pattern of the decompression sample at 1 atm. The ADXRD pattern of the decompression sample owns the same ADXRD positions with the initial sample but lower intensity, which is in sync with the incomplete recrystallization process (Fig. 7(a) and Fig. S9). The representative refinement results are shown in Fig. S8. The corresponding refinement results, including cell volume and lattice parameters, are shown in Table S2. Cell parameters and volume of β-$GeSe_2$ are decreasing monotonously before amorphization (Figs. 7(b) and 7(c)). Compared with previous reports,[37] we have a high precision and more systematic XRD measurement to obtain the accurate structural parameters of β-$GeSe_2$ at different pressures, *etc.*, providing crucial evidence to reveal the crystal lattice structure evolution of β-$GeSe_2$ under high pressure. In addition, the experimental pressure–volume (P–V) relationship is fitted using the third-order Birch-Murnaghan equation of state[21,50,51]

$$P(V) = \frac{B_0}{2}\left[\left(\frac{V_0}{V}\right)^{7/3} - \left(\frac{V_0}{V}\right)^{5/3}\right] \times \left\{1 + \frac{3}{4}(B' - 4)\left[\left(\frac{V_0}{V}\right)^{2/3} - 1\right]\right\}, \quad (2)$$

where V_0 is the atmospheric pressure volume and B_0 is the bulk modulus at ambient pressure. The fitted bulk modulus (B_0) is 22.15 GPa, which is smaller than that of other 2D layered materials such as MoSSe (31.30 GPa) and MoS_2 (47.65 GPa), suggesting a large variation in the bulk compressibility of the β-$GeSe_2$ cell under pressure.[52,53]

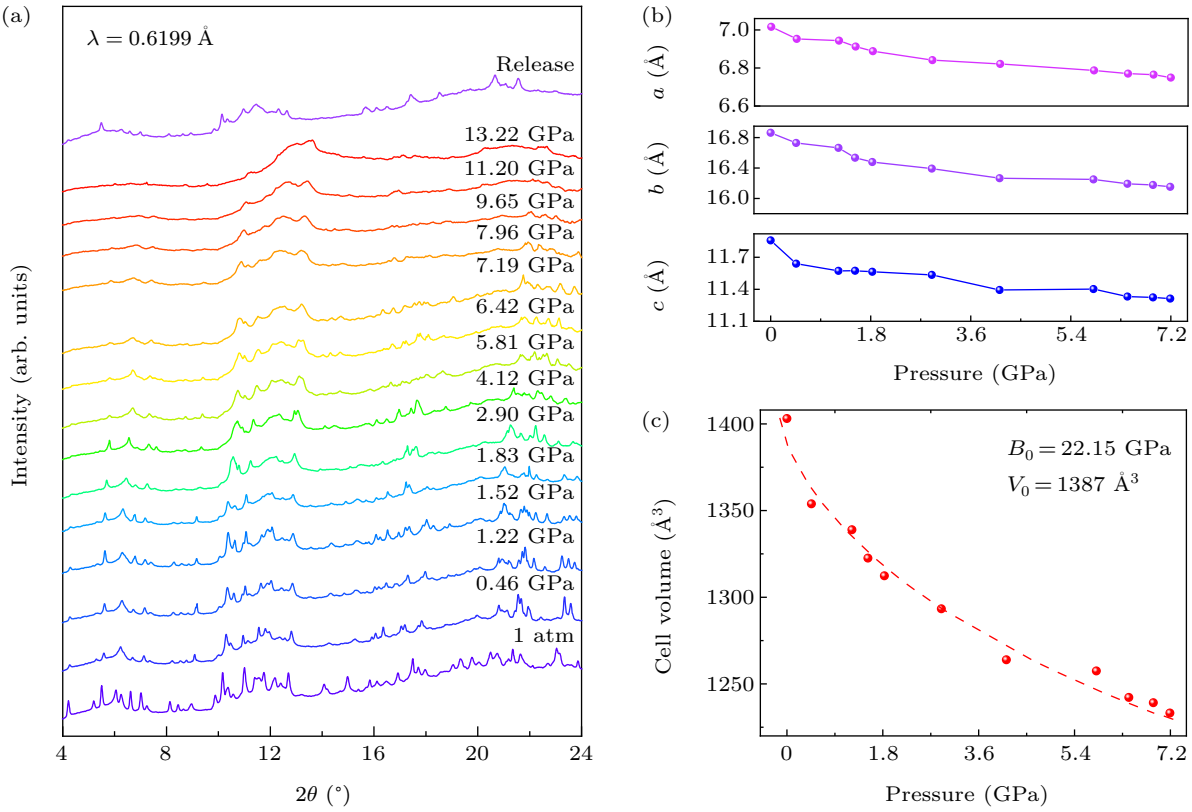


Fig. 7. (a) Representative ADXRD patterns at different pressures for β-$GeSe_2$. Pressure dependence of lattice parameters (b) and the unit cell volume (c) of β-$GeSe_2$.

3.3. Pressure regulates linearly the bandgap of β-$GeSe_2$

Our Raman and ADXRD experiments support that no structural phase transition upon compression from 1 atm to 13.80 GPa. To uncover the electronic behavior under pressure, high-pressure in situ UV-vis absorption spectroscopy was performed to understand the evolution of the electronic bandgap of β-$GeSe_2$. At atmospheric pressure, the absorption edge at 478 nm is observed,

then the absorption edge varies monotonously as pressure (Fig. 8(b)). Tauc plots of β-$GeSe_2$ at different pressures are shown in Fig. S10. Figure 8(c) shows the fitted bandgap of β-$GeSe_2$. The bandgap value of our bulk β-$GeSe_2$ under atmospheric pressure conditions is 2.59 eV, smaller than the previously reported 2.74 eV of β-$GeSe_2$.[31] This divergence could be attributed to the thickness of the sample and is in accord with the calculation result.[32,33] In Fig. 8(c), the bandgap decreases linearly to 1.65 eV when the pressure is increased to 12.16 GPa with a 0.94-eV reduction across 12.16 GPa, illustrating that the bandgap of β-$GeSe_2$ is highly tunable under pressure, which will provide new insights into the fabrication of β-$GeSe_2$-based pressure sensors and switching devices. The linear drop of the bandgap also suggests that β-$GeSe_2$ has no detectable electronic phase transition upon pressure,[21] which is in agreement with the lattice structure according to our Raman and ADXRD experimental results.

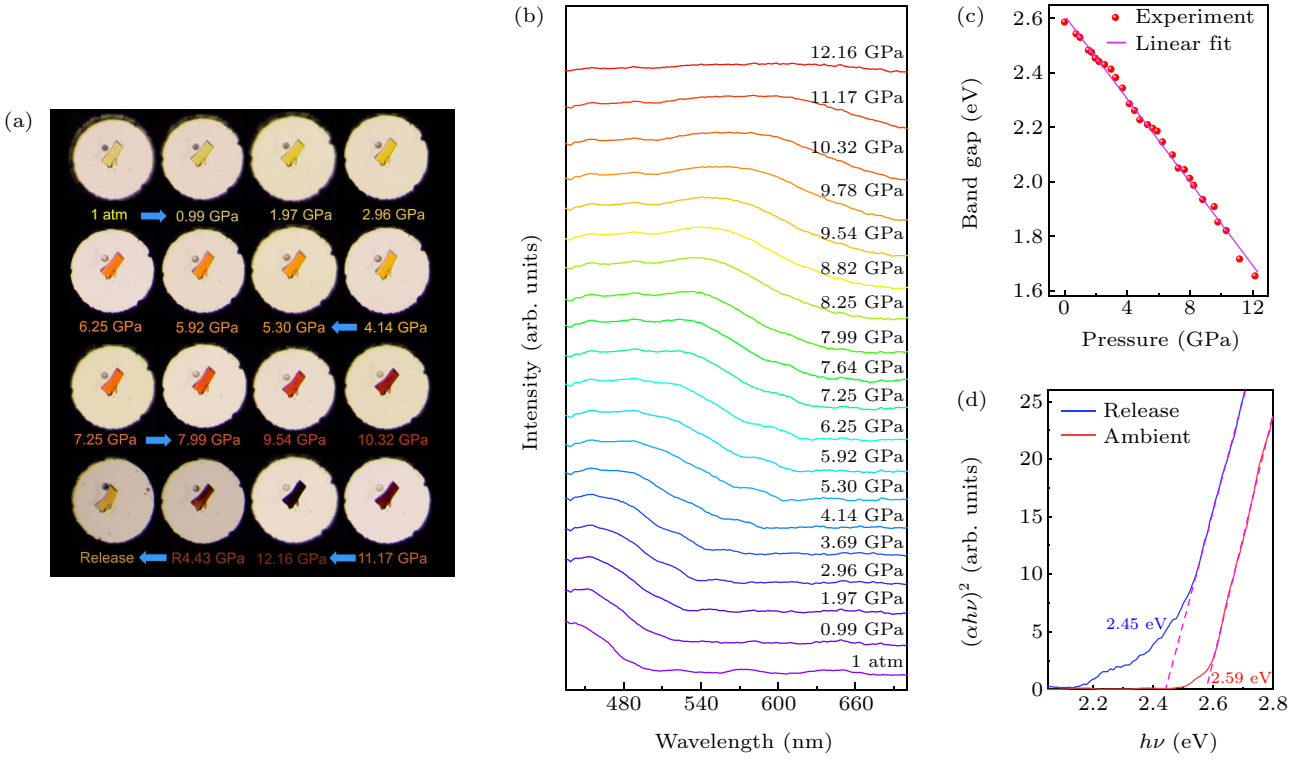


Fig. 8. (a) Optical micrograph of β-$GeSe_2$ piezochromic phenomenon upon compression and decompression. (b) and (c) Selected optical absorption spectra and bandgap evolutions of β-$GeSe_2$ as a function of pressure during pressurization. (d) Direct bandgap Tauc plots of β-$GeSe_2$ were collected at ambient pressure (red) and decompression (blue).

Figure 8(a) shows the color changing of the β-$GeSe_2$ sample under pressure during the high-pressure *in situ* UV-vis absorption experiment. At ambient pressure, the sample is transparent with the color of light yellow. As the pressure keeps increasing, the color of the sample gradually turns to dark red, and finally changes to black and opaque at 12.16 GPa completely. After pressure was released, the sample returned to the transparent state with yellow color instead of light yellow. Meanwhile, the sample recovered to a bandgap of 2.45 eV smaller than the initial 2.59 eV after decompression (Fig. 8(d) and Fig. S11), which is attributed to the incomplete recrystallization of β-$GeSe_2$.[21] When the sample was pressed to 14.01 GPa, it turns into an amorphous state and the color of the decompression sample is dark red not the yellow color of the decompression sample from the no amorphous state (Fig. S12). Although the sample became amorphous, it still owns its unique crystal structure,[42] which is verified by the partial bandgap of 2.13 eV of the decompression sample (Fig. S13).

4. Conclusion

In summary, we have systematically and comprehensively investigated the crystal structure and bandgap evolution of the 2D semiconductor β-$GeSe_2$ under high pressure. According to our high-precise ULF Raman scattering measurement and high-resolution synchrotron radiation x-ray diffraction results, there is no obvious structural phase transition during the pressurization up to 13.22 GPa. Some disorder exists above 6.91 GPa, which could be well supported by the FWHM collective broaden of phonons above 6.91 GPa in Raman spectra. The inconformity in the energy between 210-cm^{-1} and 216-cm^{-1} phonons above 6.91 GPa suggests that interlayer spacing decreasing induced by pressure along the *c* axis has a more obvious effect on the phonon energy than Ge–Se bond breaking. This indirectly supports that the partial breaking of the Ge–Se bond would not induce a macroscopically structural deformation. Based on the same response to pressure, the anomaly at 6.91 GPa in 196-cm^{-1} phonon energy is considered with the same origin as the 210-cm^{-1} phonon, both of

which are attributed to the Ge–Se bond of tetrahedral breaking. The reason for the continuous softening of 151-cm^{-1} and 167-cm^{-1} Raman peaks with pressure is interpreted by the weak of intramolecular bonds. Apart from lattice information, for electronics, the bandgap could be continuously modulated from 2.59 eV to 1.65 eV as pressure changing from 1 atm to 12.16 GPa, accompanied by the sample color varying from shiny yellow to black. If the sample is not pressed into an amorphous state, the ADXRD patterns and bandgap results both support that β-$GeSe_2$ shows an incomplete recrystallization process when the sample be completely decompressed. These research results refresh the fundamental understanding of the structure and bandgap of β-$GeSe_2$ and can provide some insights into the pressure domination of the structural and optoelectronic properties of 2D Ge-based binary materials.

Acknowledgments

Project supported by the National Natural Science Foundation of China (Grant Nos. 12004339, 11874328, 11904322, 61804047, 22071221, and 21905252), China Postdoctoral Science Foundation (Grant Nos. 2018M640679 and 2019T120629), and the Zhongyuan Academician Foundation (Grant No. ZYQR201810163).

References

[1] Geim A K and Grigorieva I V 2013 *Nature* **499** 419
[2] Wu J B, Lin M L, Cong X, Liu H N and Tan P H 2018 *Chem. Soc. Rev.* **47** 1822
[3] Tan C L, Cao X H, Wu X J, He Q Y, Yang J, Zhang X, Chen J Z, Zhao W, Han S K, Nam G H, Sindoro M and Zhang H 2017 *Chem. Rev.* **117** 6225
[4] Cai Z Y, Liu B L, Zou X L and Cheng H M 2018 *Chem. Rev.* **118** 6091
[5] Xia F N, Wang H, Xiao D, Dubey M and Ramasubramaniam A 2014 *Nat. Photon.* **8** 899
[6] Pang Y D, Wu E X, Xu Z H, Hu X D, Wu S, Xu L Y, and Liu J 2021 *Chin. Phys. B* **30** 68501
[7] Wang Y, Kim J C, Wu R J, Martinez J, Song X J, Yang J, Zhao F, Mkhoyan K A, Jeong H Y and Chhowalla M 2019 *Nature* **568** 70
[8] Roy T, Tosun M, Kang J S, Sachid A B, Desai S B, Hettick M, Hu C M C and Javey A 2014 *ACS Nano* **8** 6259
[9] Mak K F and Shan J 2016 *Nat. Photon.* **10** 216
[10] Guo J, Liu Y, Ma Y, Zhu E B, Lee S, Lu Z X, Zhao Z P, Xu C H, Lee S J, Wu H, Kovnir K, Huang Y and Duan X F 2018 *Adv. Mater.* **30** 1705934
[11] Jin H Y, Guo C X, Liu X, Liu J L, Vasileff A, Jiao Y, Zheng Y and Qiao S Z 2018 *Chem. Rev.* **118** 6337
[12] Li W B, Qian X F and Li J 2021 *Nat. Rev. Mater.* **6** 829
[13] Wang X S, Song Z G, Wen W, Liu H N, Wu J X, Dang C H, Hossain M, Iqbal M A and Xie L M 2019 *Adv. Mater.* **31** 1804682
[14] Ma X L, Zhang R J, An C H, Wu S, Hu X D and Liu J 2019 *Chin. Phys. B* **28** 037803
[15] Wang Y, Xiao J, Zhu H Y, Li Y, Alsaid Y, Fong K Y, Zhou Y, Wang S Q, Shi W, Wang Y, Zettl A, Reed E J and Zhang X 2017 *Nature* **550** 487
[16] Voiry D, Mohite A and Chhowalla M 2015 *Chem. Soc. Rev.* **44** 2702
[17] Kappera R, Voiry D, Yalcin S E, Branch B, Gupta G, Mohite A D and Chhowalla M 2014 *Nat. Mater.* **13** 1128
[18] Voiry D, Yamaguchi H, Li J W, Silva R, Alves D C B, Fujita T, Chen M W, Asefa T, Shenoy V B, Eda G and Chhowalla M 2013 *Nat. Mater.* **12** 850
[19] Wang L R, Yao P P, Wang F, Li S F, Chen Y P, Xia T Y, Guo E J, Wang K, Zou B and Guo H Z 2020 *Adv. Sci.* **7** 1902900
[20] Guo S H, Zhao Y S, Bu K J, Fu Y P, Luo H, Chen M T, Hautzinger M P, Wang Y Q, Jin S, Yang W G and Lu X J 2020 *Angew. Chem. Int. Ed.* **59** 17533
[21] Geng T, Ma Z, Chen Y, Cao Y, Lv P, Li N and Xiao G 2020 *Nanoscale* **12** 1425
[22] Zhang L L, Tang Y L, Khan A R, Hasan M M, Wang P, Yan H, Yildirim T, Torres J F, Neupane G P, Zhang Y P, Li Q and Lu Y R 2020 *Adv. Sci.* **7** 2002697
[23] Guo S H, Bu K J, Li J W, Hu Q Y, Luo H, He Y H, Wu Y H, Zhang D Z, Zhao Y S, Yang W G, Kanatzidis M G and Lu X J 2021 *J. Am.Chem. Soc.* **143** 2545
[24] Oliva R, Laurien M, Dybala F, Kopaczek J, Qin Y, Tongay S, Rubel O and Kudrawiec R 2019 *npj 2D Mater. Appl.* **3** 20
[25] Chi Z H, Zhao X M, Zhang H, Goncharov A F, Lobanov S S, Kagayama T, Sakata M and Chen X J 2014 *Phys. Rev. Lett.* **113** 036802
[26] Zhuang Y K, Dai L D, Wu L, Li H P, Hu H Y, Liu K X, Yang L F and Pu C 2017 *Appl. Phys. Lett.* **110** 122103
[27] Wang P, Wang Y G, Qu J Y, Zhu Q, Yang W G, Zhu J L, Wang L P, Zhang W W, He D W and Zhao Y S 2018 *Phys. Rev. B* **97** 235202
[28] Nayak A P, Bhattacharyya S, Zhu J, Liu J, Wu X, Pandey T, Jin C Q, Singh A K, Akinwande D and Lin J F 2014 *Nat. Commun.* **5** 3731
[29] Yang Y S, Liu S C, Li Z B, Xue D J and Hu J S 2021 *Chem. Commun.* **57** 565
[30] Zhou X, Hu X Z, Zhou S S, Zhang Q, Li H Q and Zhai T Y 2017 *Adv. Funct. Mater.* **27** 1703858
[31] Yang Y S, Liu S C, Yang W, Li Z B, Wang Y, Wang X, Zhang S S, Zhang Y, Long M S, Zhang G M, Xue D J, Hu J S and Wan L J 2018 *J. Am.Chem. Soc.* **140** 4150
[32] Yang Y S, Wang X, Liu S C, Li Z B, Sun Z Y, Hu C G, Xue D J, Zhang G and Hu J S 2019 *Adv. Sci.* **6** 1801810
[33] Yan Y, Xiong W, Li S, Zhao K, Wang X, Su J, Song X, Li X, Zhang S, Yang H, Liu X, Jiang L, Zhai T, Xia C, Li J and Wei Z 2019 *Adv. Opt. Mater.* **7** 1900622
[34] Sabapathy T, Kiran M S R N, Ayiriveetil A, Kar A K, Ramamurty U and Asokan S 2013 *Opt. Mater. Express* **3** 684
[35] Yao J D, Liu Y L, Guo W X, Niu X Y, Li M G, Wu X X, Yu Y, Yan X Y, Xing B R, Zhang S C, Sha J and Wang Y W 2020 *Appl. Phys. Lett.* **117** 153104
[36] Popovic Z V, Jaksic Z, Raptis Y S and Anastassakis E 1998 *Phys. Rev. B: Condens. Matter* **57** 3418
[37] Grzechnik A, Grande T and Stolen S 1998 *J. Solid State Chem.* **141** 248
[38] Fuentes-Cabrera M, Wang H and Sankey O F 2002 *J. Phys. Condens. Matter* **14** 9589
[39] Durandurdu M 2005 *Phys. Status Solidi B* **242** 3085
[40] Huang X L, Li F F, Huang Y P, Wu G, Li X, Zhou Q, Liu B B and Cui T 2016 *Chin. Phys. B* **25** 037401
[41] Song J Y, Fei G, Liu X B, Duan S, Yang B C, Chen X, Singh D J, Liu Y X, Yang L X, Guo J G and Zhang P 2020 *J. Mater. Chem. A* **8** 20054
[42] Rouss Ea U D L, Bauman R P and Porto S 1981 *J. Raman Spectrosc.* **10** 253
[43] Popoviá Z V and Stolz H J 1981 *Phys. Stat. Sol.* **108** 153
[44] Inoue K, Matsuda O and Murase K 1991 *Solid State Commun.* **79** 905
[45] Ren X, Duan L, Hu Y, Li J, Zhang R, Luo H, Dai P and Li Y 2015 *Phys. Rev. Lett.* **115** 197002
[46] Wang X D, Tan J L, Han C Q, Wang J J, Lu L, Du H C, Jia C L, Deringer V L, Zhou J and Zhang W 2020 *ACS Nano* **14** 4456
[47] Popovic Z V, Holtz M, Reimann K and Syassen K 1996 *Phys. Status Solidi B* (Germany) **198** 533
[48] Kundu A, Tristant D, Sheremetyeva N, Yoshimura A, Dias A T, Hazra K S, Meunier V and Puech P 2020 *Nano Lett.* **20** 5929
[49] Bridenbaugh P M, Espinosa G P, Griffiths J E, Phillips J C and Remeika J P 1979 *Phys. Rev. B* **20** 4140
[50] Dong Z H, Zhuravlev K K, Morin S A, Li L S, Jin S and Song Y 2012 *J. Phys. Chem. C* **116** 2102
[51] Chen B J, Deng Z, Wang X C, Feng S M, Yuan Z, Zhang S J, Liu Q Q and Jin C Q 2016 *Chin. Phys. B* **25** 077503
[52] Bera A, Singh A, Sorb Y A, Jenjeti R N, Muthu D V S, Sampath S, Narayana C, Waghmare U V and Sood A K 2020 *Phys. Rev. B* **102** 014103
[53] Chi Z H, Zhao X M, Zhang H, Goncharov A F, Lobanov S S, Kagayama T, Sakata M and Chen X J 2014 *Phys. Rev. Lett.* **113** 036802